

Supercapacitance Performances of Electrodeposited Nickel Oxide/Graphene Nanocomposite

Chunxiao Yin^{1,2}, Wencheng Wan^{1,3}, Hui Xie¹, Wenju Weng², Guangjiu Li², Binghang Li¹, Yubao Wang¹, Xianqun Wu¹, Wei Sun^{1,*}

¹ Key Laboratory of Laser Technology and Optoelectronic Functional Materials of Hainan Province, College of Chemistry and Chemical Engineering, Hainan Normal University, Haikou 571158, P R China

² College of Chemistry and Molecular Engineering, Qingdao University of Science and Technology, Qingdao 266042, P R China

³ Key Laboratory of Marine Environmental Corrosion and Bio-fouling, Institute of Oceanology, Chinese Academy of Sciences, Qingdao 266071, China

*E-mail: sunwei@qust.edu.cn

Received: 10 October 2018 / Accepted: 5 March 2019 / Published: 10 April 2019

In this paper graphene (GR) was obtained by electrochemical reduction of graphene oxide on the surface of nickel foam (NF). Then NiO nanocrystals were obtained on the GR/NF surface by electrochemical method to get NiO/GR/NF electrode, which was characterized by scanning electron microscopy (SEM). Various electrochemical methods such as cyclic voltammetry, AC impedance, constant current charge and discharge were used to test the electrochemical performances of the electrode. The results indicated that the capacitive properties of the composite were improved effectively due to the presence of nanometer-sized NiO and GR, and the specific capacitance of the composite was calculated as 381 mF/cm² at current density of 1 mA/cm². The specific capacitance retention rate of 1000 cycles at high current density was 97.4% with good cycle stability, which indicated that NiO/GR composite could be used as good supercapacitor material.

Keywords: Nickel oxide, Graphene, Nanocomposite, Supercapacitors, Electrochemistry.

1. INTRODUCTION

Supercapacitors are currently attracting intensive attentions due to the superior characteristics including excellent recycling performance, fast charge and discharge ability, large specific capacitance and less environmental pollution. Electrode materials are the main factor that affect the performance of supercapacitor, of which capacitance mainly originates from the surface reaction [1-4], such as the surface charge separation at the interface of electrode/electrolyte and surface faradic redox reactions [5, 6].

Recently transition metal oxides are widely reported in the fabrication of supercapacitor, which exhibit large energy density than double layer capacitors [7, 8]. Noble metal oxides including RuO₂ and IrO₂ show excellent properties and act as pseudocapacitive electrode materials, which are limited to be used due to its expensive cost [9]. Pseudo capacitive properties of base metal oxides including the oxides of Mn [10], Co [11], Zn [12], Fe [13], Ni [14-16] etc. have attracted extensive attentions. As an ideal pseudo capacitor material, nickel oxide (NiO) has many advantages such as low price, easy preparation and high specific capacitance [2]. Various methods including hydrothermal, solvothermal, chemical precipitation, sol-gel, electrodeposition and microwave assisted method have been devised for the synthesis of NiO. The differences of morphology and structures of NiO materials result in the changes of their capacitance properties. For examples, Yuan et al. prepared porous net-like Ni(OH)₂/NiOOH composite film by chemical bath deposition with the specific capacitance as 1420 F/g [17]. Srinivasan et al. prepared a NiO porous thin film electrode by electrochemical method with the specific capacitance of 59 F/g [18]. However, NiO exhibits some disadvantages such as poor electronic conductivity, narrow electrochemical window, low power and energy density, which make it difficult to achieve high theoretical specific capacitance. In order to improve the conductivity and energy density, NiO can be combined with other materials to obtain synergetic conductivity and stability. Zhao et al. fabricated a two-dimensional graphene (GR) and NiO composite with the specific capacitance of 525 F/g [19]. Su et al. used NiO and commercial carbon nanotubes as electrode materials for electrochemical capacitors with the specific capacitance of 328 F/g [20]. Zheng et al. prepared a porous NiO/multi-walled carbon nanotube composite electrode by homogeneous liquid precipitation, which exhibited the specific capacitance of 206 F/g [21]. Fang et al. prepared Ni(OH)₂ and reduced graphene oxide composite by hydrothermal method with the specific capacitance of 2134 F/g [22].

In this paper electrochemical reduction was adopted to deposit GR on the nickel foam (NF) collector surface with further deposition of NiO to get a NiO/GR/NF nanocomposite, which was characterized by scanning electron microscopy. The capacitor performance of this nanocomposite on the electrode was carefully investigated by various electrochemical methods.

2. EXPERIMENTAL

2.1 Instruments

A CHI 660E electrochemical workstation (Shanghai CH Instrument, China) was used for electrochemical experiments, which was connected with a modified NF electrode (1.0 × 1.0 cm²) as working electrode. Scanning electron microscopy (SEM) was performed on a JSM-7100F scanning electron microscope (JEOL, Japan).

NF (Kunshan Guangjiayuan New Mater. Ltd. Co., China) and graphene oxide (GO, purity > 99%, Shanxi Institute of Coal Chemistry, Chinese Academy of Sciences, China) were used as received. The purity of the reagents was of analytical grade with redistilled water used throughout.

2.2 Preparation of the nanocomposite

The preparation of GR/NF electrode was described with following steps. Firstly NF was put in acetone and 1.0 mol/L HCl solution respectively with ultrasonic clean for 10 min in per solution, then it was washed thoroughly with water and dried with N₂ gas. Afterwards NF (size 1.0×1.0 cm²) was immersed into a 1.0 mg/mL GO solution (in pH = 8.0 deoxygenate PBS) and electrodeposition method was taken place by constant potential reduction at -1.2 V for 600 s. Then NF was taken out, washed with water and dried in vacuum to get a GR/NF electrode.

The fabrication process of NiO/GR/NF nanocomposite was performed as follows. The newly prepared GR/NF electrode was immersed in a 1.0 mol/L Ni(NO₃)₂ solution with pH 4.0 acetic acid and cyclic voltammetric scan was operated in the potential window from -1.0 V to 0.5 V at scan rate of 70 mV/s for 30 cycles. Then the electrochemical window was set from -1.0 V to 1.5V with the scan rate of 100 mV/s for 30 cycles in pH 7.0 PBS to get NiO/GR/NF electrode, which was taken out and dried at room temperature.

2.3 Characterization of the nanocomposite

SEM was applied to observe the surface morphology and microscopic structure of nanocomposite on the electrode surface. Electrochemical tests including cyclic voltammetry, constant current charging and discharging were performed with a three-electrodes system, which was consisted of the nanocomposite as working electrode, Pt wire electrode as counter electrode and Hg/HgO electrode as reference electrode with 1.0 mol/L KOH solution as the electrolyte. The potential window of cyclic voltammetry was from 0 to 0.8 V and the current density of the galvanostatic charge/discharge curve was from 1.0 mA/cm² to 40.0 mA/cm².

3. RESULTS AND DISCUSSION

3.1 Characteristics of the modified electrode

SEM image of NF (Fig.1A) gave a typical 3D macrostructure with a flat surface. GO was in negative charges and could be electrochemically deposited on NF surface under electric field force. Then it would release electron over the positive NF electrode and reduced to GR [23]. The electrodeposited GR layer was thin and the morphology on the surface of NF hadn't changed significantly after deposition (Fig. 1B) comparing to the bare Ni foam (Fig. 1A). However, it is clear that there is coating layer present on NF at the high magnification SEM image (Fig. 1B), indicating the successful deposition of GR on NF surface. On electrodeposited GR/NF, a uniformly GR layer could be found with a typical wrinkle appearance (inset of Fig.1B), which could effectively improve the interfacial conductivity. Xia et al. reported the NF covered by the similarly wrinkled GR sheet with the **electrophoretic deposition** method [24]. After the further deposition of NiO, it can be seen that NiO nanostructures successfully coated on the entire surface area of GR/NF and a roughness interface could be observed with many small particles appeared, which increased the effective surface area

greatly. Therefore, the contact of electrolyte with the electrode surface was sufficient, which was benefit to promote the transfer of electrons and electrolyte ions effectively. This unique structure and morphology made it useful in electrochemical capacitors, leading to pseudocapacitance when ions were adsorbed onto the surface of the samples and thereby improving capacitive behavior.

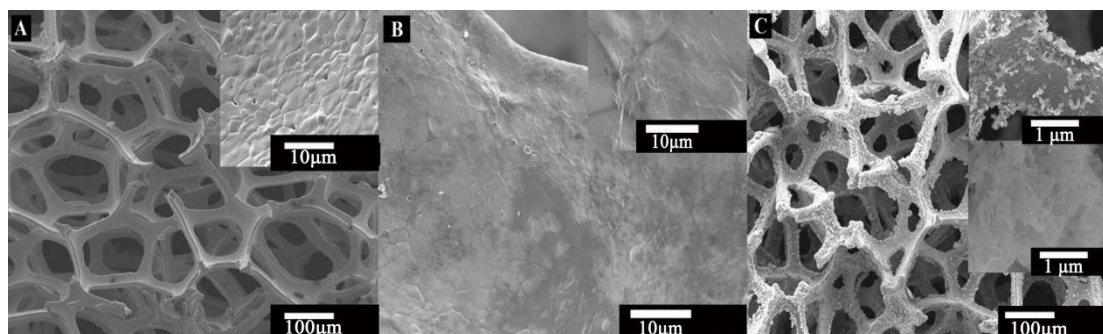


Figure 1. SEM images of (A) NF, (B) GR/NF and (C) NiO/GR/NF with enlarged images inset.

3.2 Cyclic voltammetric results

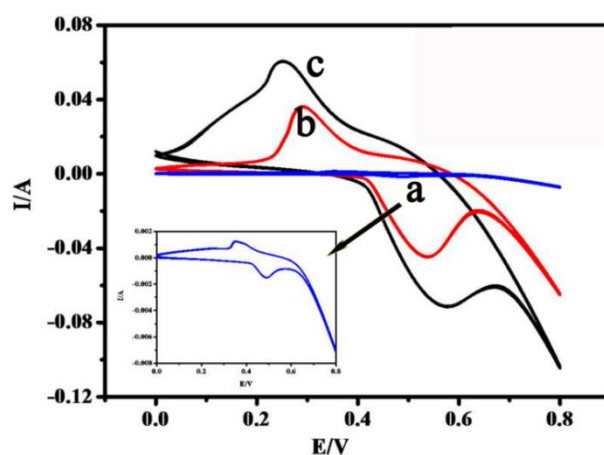


Figure 2. Cyclic voltammetric curves of (a) NF, (b) GR/NF and (c) NiO/GR/NF in a 1.0 mol/L KOH solution at the scan rate of 100 mV/s, (inset was the enlarged view of curve a).

Cyclic voltammetric curves of different electrodes at the scan rate of 100 mV/s in a 1.0 mol/L KOH solution were shown in Fig.2. The shapes of curves with two redox peaks differed from those of ideal electrochemical double-layer capacitance, indicating the pseudocapacitive behavior of the electrode materials [25, 26]. As for NF electrode (curve a and inset of Figure 2), the smallest redox peak currents appeared due to the existence of NiO that formed by oxidation process in air on the surface of the as-cleaned NF that contributed to the capacitance [27]. On GR/NF (curve b), the redox peak currents increased greatly, which was attributed to the presence of GR nanosheet on NF surface that enhanced the capacitive current, and the increased area exhibited typical double-layer capacitance performance. Notably, the redox peak of Ni(OH)₂ with high pseudocapacitance would embosk the rectangular shape of GR with double layer capacitance, which is similar to the previous reports [28].

On the surface of Ni-based electrodes, nickel hydroxide (NiOOH) would be formed from redox process between NiO and NiOOH in the alkaline environment, which could be explained using the following equation: $\text{NiO} + \text{OH}^- \leftrightarrow \text{NiOOH} + \text{e}^-$ [29]. On NiO/GR/NF (curve c), the biggest redox peak currents appeared, indicating the presence of NiO further increased the interfacial capacitance. The presence of GR nanosheets on NF resulted in a higher conductive interface and was benefit for the further deposition of nanosized NiO. GR can provide more sites, large surface area and high conductive interface for deposition of nanosized NiO, and the formed nanocomposite exhibited synergistic effects for the pseudocapacitive performance [30].

3.3 Optimization of NiO deposition

Nano-NiO was electrodeposited on GR/NF electrode by cyclic voltammetry, and different amounts quantities of nano-NiO on the surface of GR/NF were optimized by changing the number of scan cycles. Furthermore, the formation and performances of NiO/GR/NF were checked by cyclic voltammetry in a 1.0 mol/L KOH aqueous solution. As shown in Fig.3A, the increase of cyclic scans resulted in the more deposited amount of NiO and the maximum area of cyclic voltammogram appeared at the number of 30 scan cycles, indicating that the formed NiO/GR/NF with 30 deposition cycles had the largest specific capacitance. Further increase of scan cycles led to the decrease of the area of cyclic voltammogram, which indicated that the increase of the thickness of NiO film was not benefit for the capacitance due to the decrease of the active surface contacted with electrolyte [31]. Galvanostatic charge/discharge curves of NiO/GR nanocomposites with different number of deposition cycles were checked with results shown in Fig.3B and Fig.3C. The variation curves of specific capacitance were calculated by constant current discharge curve under different current densities. The shoulders in the Fig.3B at 0.45 V during charging and 0.30 V during discharging indicated the redox reactions, which was in consistent with the literature report [29]. The results in Fig.3B and Fig.3C also showed that the largest specific capacitance was got at 30 cycles of the deposition, which were in agreement with CV analysis. Therefore, the preparation of NiO/GR/NF electrode in this experiment was optimized at the number of 30 cycles.

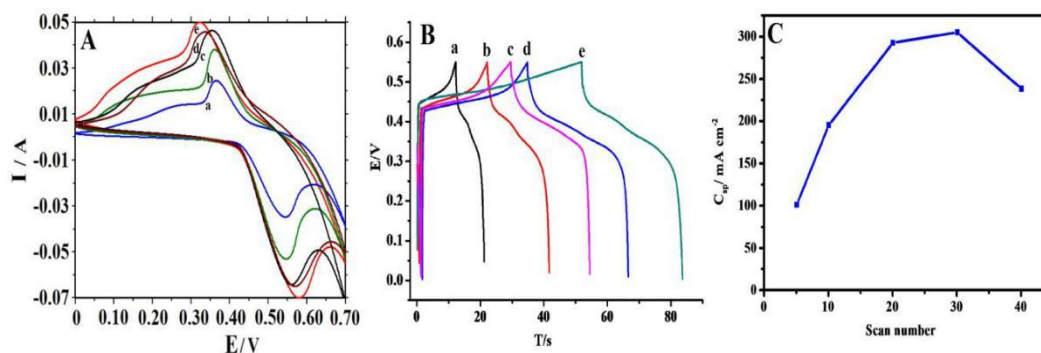


Figure 3. (A) Cyclic voltammograms of NiO/GR/NF in 1.0 mol/L KOH solution after different cyclic voltammetric cycles (from a to e: 5, 10, 40, 20, 30) with the scan rate of 100 mV/s), (B) Charge/discharge curves with the current density as 10 mA/cm², (C) Relationship of specific capacitance of NiO/GR/NF with cyclic voltammetric cycles.

3.4 Effect of scan rate

Effect of scan rate on cyclic voltammetric responses of NiO/GR/NF was shown in Fig.4, which gave a pair of redox peaks at various scan rates in the range from 5 to 150 mV/s. The redox peaks were attributed to the oxidation/reduction of NiO on the electrode surface, which was clearly identified during the cyclic sweeps and the shapes were different from those of the electric double layer capacitance. Two strong peaks were corresponded to pseudocapacitance characteristics derived from the faradic oxidation/reduction reactions and the electrode capacitance was dominated by the following interfacial redox reaction: $\text{NiO} + \text{OH}^- \leftrightarrow \text{NiOOH} + \text{e}^-$ [29]. Also, the increase of scan rate resulted in the enhancement of redox peak current, which suggested rapid diffusion-controlled electrolyte ion transport kinetics at the interface [32]. Moreover, anodic and cathodic peaks shifted toward positive and negative potentials with the increase of scan rate, which was due to the increase in electron hopping resistance to ion and electron transfer at higher scan rates [33]. At the low scan rate, slow movement of ions (OH^-) from electrolyte resulted in high utilization of electrochemically active components, therefore the charge and discharge processed completely. The increase of scan rate speeded up the movement of ions into the electrode with more ions needed, which resulted in the electrode polarization effect and irreversible reactions at a higher scan rate [34]. In addition, the redox peaks were maintained at different scan rates and the shapes of these curves were similar, meaning that the capacitive behavior of the electrode was maintained over this range [35].

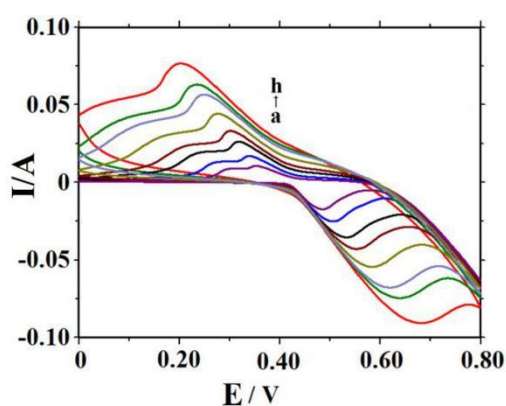


Figure 4. Cyclic voltammograms of NiO/GR/NF in 1.0 mol/L KOH solution with different scan rates (from a to h: 5, 10, 20, 30, 50, 80, 100, 150 mV/s)

3.5 Discharging curves under different current densities

Figure 5A compared the first discharge curves of NiO/GR/NF under different current densities and showed nonlinear behavior with obvious voltage plateaus appeared in all discharge curves, which gave a typical characteristic of Faraday pseudo-capacitance [36]. These were in agreement with the cyclic voltammogram in Fig. 4. With the increase of discharge current density, the discharge time of NiO/GR/NF electrode was shortened, which was caused by the increase of current density that increased charge transfer rate in electrode and electrolyte. The relationship of specific capacitance

under different discharge current densities was shown in Fig.5B. The specific capacitance can be calculated by the following equation [37]: $C = \frac{I\Delta t}{S\Delta V}$, where C (mF/cm^2) is the specific capacitance, I (mA) is the discharging current, Δt (s) is the discharging time, ΔV (V) represents the discharging potential range and S (cm^2) is the area of electrode, respectively. When the discharge current density was $1 \text{ mA}/\text{cm}^2$, the specific capacitance of NiO/GR/NF reached $381 \text{ mF}/\text{cm}^2$, and the specific capacitance was $210 \text{ mF}/\text{cm}^2$ when the current density increased to $40 \text{ mA}/\text{cm}^2$. Notably, with the 40-fold enhancement in the discharge current density, the specific capacitance remained more than 55%, indicating the unusual rate capability of the hybrid electrode [38]. An increase in current density resulted in a gradual decrease in discharge specific capacitance values, which was probably due to the resistance of NiO/GR/NF foam and the deficient Faradic redox reaction at a higher current density [39]. Furthermore, the change was attributed to the adsorption of OH^- that aggregated on the electrode surface in a short time with a large current density of charge process, which caused the decrease of OH^- concentration between electrode and electrolyte, then increased the polarization phenomenon by liquid phase diffusion on the surface of electrode. Therefore, the specific capacitance decreased with the potential increased.

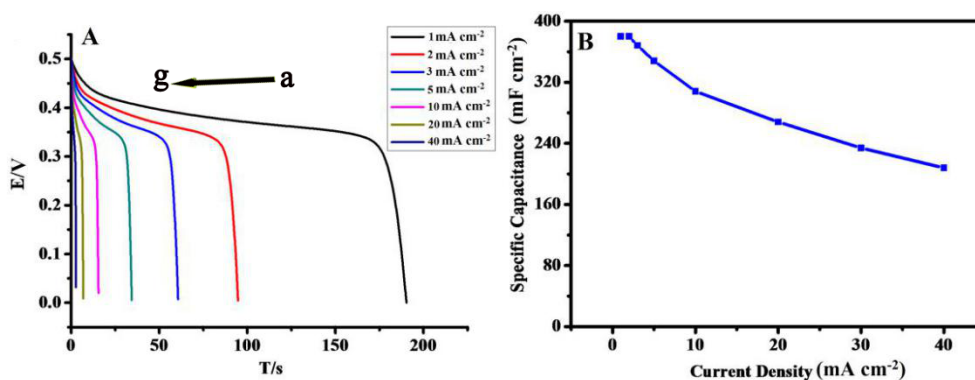


Figure 5. (A) Discharge curves under different current densities (from a to g: 1, 2, 3, 5, 10, 20, 40 mA/cm^2); (B) Specific capacitance variation curve under different current densities (1, 2, 3, 5, 10, 20, 40 mA/cm^2).

3.6 Stability

Cycling stability of electrode materials is an important factor for practical applications of supercapacitors. As shown in Fig. 6, cycling stability of NiO/GR/NF was measured by galvanostatic charge/discharge measurements in 1.0 mol/L KOH solution. The specific capacitance changes of NiO/GR/NF electrode at 1000 charge/discharge cycles test under the current density of $10 \text{ mA}/\text{cm}^2$ was exhibited with the inset of Figure 6 as partial charge/discharge curve. The similar shape of specific capacitance change curves was consistent with the previous reports [40]. The initial specific capacitance of the electrode material was $308 \text{ mF}/\text{cm}^2$ and decreased to $300.8 \text{ mF}/\text{cm}^2$ after 1000 cycle charge/discharge with 97.4% remained, indicating the high specific capacitance at high current density with excellent cycling stability [41]. The specific capacitance of NiO/GR/NF was compared with other

electrode materials and shown in Table 1 [42-45], which proved that NiO/GR/NF was a good electrode material for supercapacitor.

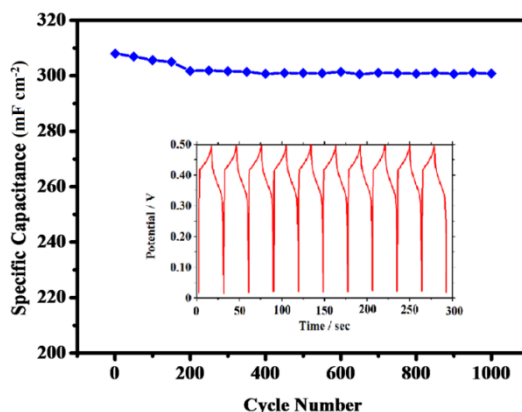


Figure 6. Cyclic charge/discharge specific capacitance curve at 1000 cycles with current density of 10 mA/cm² (inset cyclic charge/discharge curves).

Table 1. Comparison of specific capacitance of different electrode materials

Electrode materials	Electrolyte	Specific capacitance	Current density (mA/cm ²)	References
SiCNWs@Fe ₂ O ₃ NNAs	2 mol/L KOH	1000 mF/cm ²	2.8	[42]
Porous graphenenetworks/NF	6 mol/L KOH	183.2 mF/cm ²	1.0	[43]
NiO/MoO ₂ composite	2 mol/L KOH	600 mF/cm ²	2.0	[44]
Hierarchical mesoporous graphene and ternary nickel cobalt sulfide (Ni-Co-S) arrays	6 mol/L KOH	9200 mF/cm ²	100	[45]
NiO/GR/NF	1 mol/L KOH	381.0 mF/cm ²	1.0	This work

4. CONCLUSION

In this paper, NF was used as the basic electrode for the further electrodeposition of GR and NiO to get NiO/GR/NF. Scanning electron microscopic results showed that GR and NiO were uniformly coated on the skeleton of NF. Electrochemical tests indicated that the capacitance of NiO/GR nanocomposite gave the highest value due to the simultaneous presence of NiO and GR on the NF surface, which effectively improved the capacitance performance due to the synergetic effects. The charge-discharge test showed that the specific capacitance of NiO/GR nanocomposites at 1 mA/cm² current density was 381 mF/cm². After the 1000 charge/discharge cycles, cycling stability was

good and the specific capacitance retention rate was 97.4% at high current density of 10.0 mA/cm². Therefore, NF provided a three-dimensional structure with good stability and large surface area, which was benefit for the formation of GR and NiO nanocomposite on its surface with improved capacitive performance and NiO/GR/NF acted as excellent electrode material for supercapacitor.

ACKNOWLEDGEMENTS

This project was supported by Hainan Provincial Natural Science Foundation of China (2017CXTD007), the Key Science and Technology Program of Haikou City (2017042) and Foundation of Key Laboratory of Sensor Analysis of Tumor Marker of Ministry of Education of Qingdao University of Science and Technology (STAM201808).

References

1. Y.Y. Wang, Y.Y. Xia, *Adv. Mater.*, 25 (2013) 5336.
2. M.M. Sk, C.Y. Yue, K. Ghosh, R.K. Jena, *J. Power Sources*, 308 (2016) 121.
3. Z. Wu, L. Li, J.M. Yan, X.B. Zhang, *Adv. Sci.*, 4 (2017) 1600382.
4. T. Chen, L.M. Dai, *Mater. Today*, 16 (2013) 272.
5. J. Yan, Q. Wang, T. Wei, Z.J. Fan, *Adv. Energy Mater.*, 4 (2014) 1300816.
6. Y. Zhang, H. Feng, X.B. Wu, L.Z. Wang, A.Q. Zhang, T.C. Xia, H.C. Dong, X.F. Li, L.S. Zhang, *Int. J. Hydrogen Energy*, 34 (2009) 4889.
7. L. Wang, G.R. Duan, J.W. Zhu, S.M. Chen, X.H. Liu, S. Palanisamy, *J. Colloid Interf. Sci.*, 483 (2016) 73.
8. S. Ortaboy, J.P. Alper, F. Rossi, G. Bertoni, G. Salviati, C. Carraro, R. Maboudian, *Energy Environ. Sci.*, 10 (2017) 1505.
9. T.P. Gujar, V.R. Shinde, C.D. Lokhande, W.Y. Kim, K.O. Jung, O.S. Joo, *Electrochim. Commun.*, 9 (2007) 504.
10. L.Q. Mai, F. Yang, Y.L. Zhao, X. Xu, L. Xu, Y.Z. Luo, *Nat. Commun.*, 2 (2011) 381.
11. H. Cheng, Z.G. Lu, J.Q. Deng, C.Y. Chung, K.L. Zhang, Y.Y. Li, *Nano Res.*, 3 (2010) 895.
12. Y.B. He, G.R. Li, Z.L. Wang, C.Y. Su, Y.X. Tong, *Energy Environ. Sci.*, 4 (2011) 1288.
13. Q.T. Qu, S.B. Yang, X.L. Feng, *Adv. Mater.*, 23 (2011) 5574.
14. Y.T. Chu, S.L. Xiong, B.S. Li, Y.T. Qian, B.J. Xi, *ChemElectroChem*, 3 (2016) 1347.
15. J. Chang, M. Park, D. Ham, S.B. Ogale, R.S. Mane, S.H. Han, *Electrochim. Acta*, 53 (2008) 5016.
16. C.H. Wu, S.X. Deng, H. Wang, Y.X. Sun, J.B. Liu, H. Yan, *ACS Appl. Mater. Interfaces*, 6 (2014) 1106.
17. Y.F. Yuan, X.H. Xia, J.B. Wu, Y.B. Chen, J.L. Yang, S.Y. Guo, *Electrochim. Acta*, 56 (2011) 2627.
18. V. Srinivasan, J.W. Weidner, *J. Electrochem. Soc.*, 144 (1997) 210.
19. B. Zhao, J.S. Song, P. Liu, W.W. Xu, T. Fang, Z. Jiao, H.J. Zhang, Y. Jiang, *J. Mater. Chem.*, 21 (2011) 18792.
20. A.D. Su, X. Zhang, A. Rinaldi, S.T. Nguyen, H.H. Liu, Z.B. Lei, L. Lu, H.M. Duong, *Chem. Phys. Lett.*, 561 (2013) 68.
21. Y.Z. Zheng, M.L. Zhang, P. Gao, *Mater. Res. Bull.*, 42 (2007) 1740.
22. D.L. Fang, Z.D. Chen, X. Liu, Z.F. Wu, C.H. Zheng, *Electrochim. Acta*, 81 (2012) 321.
23. M. Wang, L.D. Duong, J.S. Oh, N.T. Mai, S.H. Kim, S.C. Hong, T.S. Hwang, Y.K. Lee, J.D. Nam, *ACS Appl. Mater. Interfaces*, 6 (2014) 1747.
24. X.H. Xia, J.P. Tu, Y.J. Mai, R. Chen, X.L. Wang, C.D. Gu, X.B. Zhao, *Chem. Eur. J.*, 17 (2011) 10898.
25. Y.L. Shao, M. El-Kady, L.J. Wang, Q.H. Zhang, Y.G. Li, H.Z. Wang, M.F. Mousavi, R. Kaner,

- Chem. Soc. Rev.*, 44 (2015) 3639.
26. Y.L. Chena, Y. Wanga, P. Suna, P.H. Yanga, L.H. Dua, W.J. Maia, *J. Mater. Chem. A*, 3 (2015) 20614.
 27. W. Xing, S.Z. Qiao, X.Z. Wu, X.L. Gao, J. Zhou, S.P. Zhuo, S.B. Hartono, D.H. Jurcakova, *J. Power Sources*, 196 (2011) 4123.
 28. B. Zhao, T. Wang, L. Jiang, K. Zhang, M.M.F. Yuen, J.B. Xu, X.Z. Fu, R. Sun, C.P. Wong, *Electrochim. Acta*, 192 (2016) 205.
 29. C.D. Wang, J.L. Xu, M.F. Yuen, J. Zhang, Y.Y. Li, X. Chen, W.J. Zhang, *Adv. Funct. Mater.*, 24 (2014) 6372.
 30. H.B. Wang, Q.M. Pan, X.P. Wang, G.P. Yin, J.W. Zhao, *J. Appl. Electrochem.*, 39 (2009) 1597.
 31. X.J. Ma, L.B. Kong, W.B. Zhang, M.C. Liu, Y.C. Luo, L. Kang, *Rsc Adv.*, 4 (2014) 17884.
 32. G.H. Chen, W.F. Yang, C.Q. Dong, T.Y. Kou, Q.G. Bai, H. Wang, Z.H. Zhang, *J. Mater. Chem. A*, 3 (2015) 17469
 33. Y.Q. Zhu, C.B. Cao, S. Tao, W.S. Chu, Z.Y. Wu, Y.D. Li, *Sci. Rep.*, 4 (2014) 5787.
 34. C.H. Wu, S.X. Deng, H. Wang, Y.X. Sun, J.B. Liu, H. Yan, *ACS Appl. Mater. Interfaces*, 6 (2014) 1106.
 35. L. Gu, Y.W. Wang, R. Lu, L. Guan, X.S. Peng, J. Sha, *J. Mater. Chem. A*, 2 (2014) 7161.
 36. J.L. Lv, Z.Q. Wang, H. Miura, *Solid State Commun.*, 269 (2018) 45.
 37. V.H. Nguyen, C. Lamiel, J.J. Shim, *Electrochim. Acta*, 161 (2015) 351.
 38. M. Mirzaee, C. Dehghanian, *Int. J. Hydrogen Energy*, 43 (2018) 12233.
 39. Z.Y. Lu, C. Zheng, W. Zhu, X.M. Sun, *Chem. Commun.*, 47 (2011) 9651.
 40. A. Bello, K. Makgopa, M. Fabiane, D. Dodoo-Ahrin, K. Ozoemena, N. Manyala, *J. Mater. Sci.*, 48 (2013) 6707.
 41. S.X. Wu, K. S. Hui, K. N. Hui, K.H. Kim. *J. Mater. Chem. A*, 4 (2016) 9113.
 42. J. Zhao, Z.J. Li, X.C. Yuan, Z. Yang, M. Zhang, A.L. Meng, Q.D. Li, *Adv. Energy Mater.*, 9 (2018) 1702787.
 43. S.L. Yang, B.C. Deng, R.J. Ge, L. Zhang, H. Wang, Z.H. Zhang, W. Zhu, G.Z. Wang, *Nanoscale Res. Lett.*, 9 (2014) 672.
 44. S.C. Hou, G.H. Zhang, W. Zeng, J. Zhu, F.L. Gong, F. Li, H.G. Duan, *ACS Appl. Mater. Interfaces*, 16 (2014) 13564.
 45. V. H. Nguyen, C. Lamiel, J.J. Shim, *Electrochim. Acta*, 161 (2015) 351.